Applied Surface Science 478 (2019) 459–464

Contents lists available at ScienceDirect

Applied Surface Science

journal homepage: www.elsevier.com/locate/apsusc

Full length article

First-principles study on OH-functionalized 2D electrides: Ca_2NOH and $Y_2C(OH)_2$, promising two-dimensional monolayers for metal-ion batteries

Dandan Wang[a,c,*], Haibo Li[a], Liangliang Zhang[b], Zhonghui Sun[d], DongXue Han[d,e], Li Niu[d,e], Xin Zhong[a], Xin Qu[a], Lihua Yang[a]

[a] Key Laboratory of Functional Materials Physics and Chemistry of the Ministry of Education, College of Physics, Jilin Normal University, Siping 136000, China
[b] State Key Laboratory of Luminescence and Applications, Changchun Institute of Optics, Fine Mechanics and Physics, Chinese Academy of Sciences, 3888 Eastern South Lake Road, Changchun 130033, China.
[c] National Demonstration Center for Experimental Physics Education, Jilin Normal University, Siping 136000, China
[d] Center for Advanced Analytical Science, School of Chemistry and Chemical Engineering, Guangzhou University, Guangzhou 510006, China
[e] State Key Laboratory of Electroanalytical Chemistry, c/o Engineering Laboratory for Modern Analytical Techniques, Changchun Institute of Applied Chemistry, Chinese Academy of Science, Changchun 130022, Jilin, China

ARTICLE INFO

Keywords:
OH-functionalized 2D electrides
Ca_2NOH
$Y_2C(OH)_2$
Adsorption and diffusion of metal atoms
First-principles study

ABSTRACT

We designed two stable monolayers of Ca_2NOH and $Y_2C(OH)_2$ through replacing the anionic electrons with negatively charged hydroxide ions. Calculation results indicate that these two monolayers are dynamic and thermodynamic stable. Ca_2NOH is determined as an indirect semiconductor with band gap of 1.51 eV based on hybrid functional calculations, while $Y_2C(OH)_2$ possesses a direct band gap of 0.72 eV. Moreover, to investigate the potential applications of Ca_2NOH and $Y_2C(OH)_2$ monolayers, we studied the adsorption and diffusion performance of Li, Na and Mg atoms on their surfaces. The calculated adsorption energies, differential charge density and Bader charge analysis reveal that Li, Na and Mg atoms could anchor on Ca_2NOH and $Y_2C(OH)_2$ surfaces. Nudged Elastic band calculation results suggest that the barriers for Li, Na, and Mg diffusion on Ca_2NOH surface are 0.79 eV, 0.42 eV and 0.42 eV. While $Y_2C(OH)_2$ monolayer exhibits relative low diffusion barriers of 0.60 eV, 0.26 eV and 0.10 eV for Li, Na and Mg, respectively and their corresponding diffusion coefficients are as large as 1.52×10^{-18}, 1.52×10^{-12} and 1.52×10^{-8} m^2/s. The diffusion barriers and diffusion coefficients. The appropriate adsorption energies, low diffusion barriers and relative large diffusion coefficients of Na/Mg atoms imply that Ca_2NOH and $Y_2C(OH)_2$ monolayers are promising electrode materials for the corresponding metal-ion batteries. All the results serves to modify, stabilize and understand two dimensional electrides and put their properties into practical use.

1. Introduction

2D materials have caused a great deal of attention because of their unique physical and chemical properties [1–4]. Recently, 2D electrides including X_2N (X = Ca, Sr, Ba) and Y_2C have been obtained in experiment and demonstrated to be very attractive. They possess low work function, high electron mobility and efficient charge-transfer characteristics [5,6]. And they have layered structures in which electrons act as anions localized in the 2D empty spaces confined between cation layers [7]. Previous literature reports confirmed that the anionic electron quantities confined in the 2D empty spaces are 1 and 2 per X_2N unit cell ($[X_2N]^+ \cdot e^-$) and per Y_2C unit cell ($[Y_2C]^{2+} \cdot 2e^-$), respectively [8,9]. In consideration of their excellent physical and chemical properties, more and more 2D electrides have been explored and predicted, including Sr_2P, Ba_2As, Tb_2C, CaF and so on [10,11].

With the increasing knowledge of electride materials, they have been considered in practical applications. For example, $[Ca_2N]^+ \cdot e^-$ could act as an electron donor in pinacol coupling reaction with the production of $Ca(OMe)_2$ and ammonia [12]. Both $[Ca_2N]^+ \cdot e^-$ and $[Y_2C]^{2+} \cdot 2e^-$ have been reported to be promising anode materials for Na-ion batteries based on theoretical studies [13,14]. Last year, Chen et al. prepared a multilayered electride of $[Ca_2N]^+ \cdot e^-$ pressed into the nickel foam (to avoid the contact between Ca_2N and trace moisture/oxygen) and used it as anode material of Na-ion batteries for the first time [15]. Besides, in consideration of the applications of 3D electride ($[Ca_{24}Al_{28}O_{64}]^{4+} \cdot 4e^-$), the potential applications of 2D electrides may

* Corresponding author at: Key Laboratory of Functional Materials Physics and Chemistry of the Ministry of Education, Jilin Normal University, Siping 136000, China.
E-mail addresses: mila880227@126.com (D. Wang), lihaibo@jlnu.edu.cn (H. Li), zhangliangliang@ciomp.ac.cn (L. Zhang).

https://doi.org/10.1016/j.apsusc.2019.01.256
Received 8 November 2018; Received in revised form 9 January 2019; Accepted 28 January 2019
Available online 29 January 2019
0169-4332/

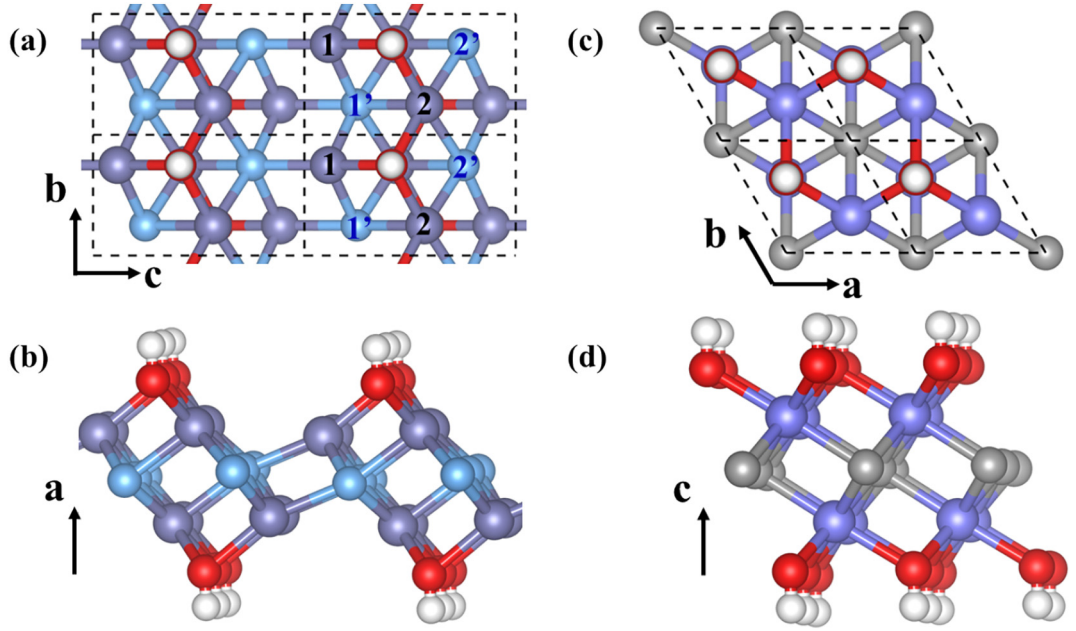

Fig. 1. Top and side views of optimized structures of (a) and (b) Ca_2NOH monolayer; (c) and (d) $Y_2C(OH)_2$ monolayer. Modena, cyan, purple, gray, red and white balls denote Ca, N, Y, C, O and H atoms, respectively. The integers of 1 and 2 in (a) indicates two unequivalent Ca atoms of Ca_1 and Ca_2, while 1′ and 2′ represent two N atoms of N_1 and N_2.

well include serving as reducing agents or catalysts for chemical reactions [16,17]. Furthermore, the monolayered or multilayered 2D electrides are more superior in practical applications [15,18,19]. Unfortunately, 2D electride monolayers and multilayers are chemically active in moisture and atmosphere, which is also discussed in recent report [20]. So Zhao et al. has applied graphane as protection layer to stabilize Ca_2N monolayer [21].

Here, we apply ourselves to enhance the stability of 2D Ca_2N and Y_2C monolayers. Inspired by element substitution strategy in material modification [22,23], what will happen if the anionic electrons of monolayered 2D electrides are replaced by hydroxyl ions? In consideration of the stoichiometric proportion and electron quantities in per Ca_2N and Y_2C unit cell, the formulas after replacement are Ca_2NOH and $Y_2C(OH)_2$. In this work we studied the structural and electronic properties of $Ca_2N(OH)$ and $Y_2C(OH)_2$ monolayers through first-principles calculations. To further exploit the application possibilities of these two novel 2D materials in metal ion batteries, their adsorption properties towards metal atoms (Li, Na and Mg) and their diffusion properties are explored.

2. Computational methods

Density functional theory (DFT) [24] using the projected augmented wave (PAW) method [25] which is implemented in the VASP package was applied in first-principles calculations. Perdew-Burke-Ernzerhof (PBE) generalized gradient approximation method [26] is employed to compute the electron exchange–correlation energy. The cutoff energy for the plane wave expansion and the convergence criterion of the forces for geometry optimizations are set as 600 eV and 0.01 eV $Å^{-1}$, respectively. The monolayer structures of Ca_2NOH and $Y_2C(OH)_2$ are derived from the original Ca_2N and Y_2C monolayers. Both the two original monolayers possess the same space group ($R\bar{3}m$) and atomic parameters as reported [5,8]. The accurate electronic band structures and density of states (DOS) for Ca_2NOH and $Y_2C(OH)_2$ monolayers are acquired based on the Heyd–Scuseria–Ernzerhof (HSE06) functional [27]. While for convenience of calculations, the DOS for adsorbed systems constructed by supercell method were calculated based on PBE functional instead of HSE06 functional. Moreover, DFT-D2 correction method of Grimme is used to take the long-range vdw interactions into consideration [28]. A 20 Å vacuum space perpendicular to the monolayer plane is employed to avoid interaction between two adjacent periodic images. A Monkhorst-Pack K-mesh for the Brillouin-zone integration with K-point separation of 0.03 $Å^{-1}$ and 0.02 $Å^{-1}$ are applied for the structure optimization and DOS calculations, respectively. Lattice dynamic stability and thermodynamic stability of Ca_2NOH and $Y_2C(OH)_2$ monolayers at room temperature were assessed based on density-functional perturbation theory (DFPT) calculations [29,30] and first-principles molecular dynamics (MD) calculations [31], respectively. The MD calculations in NVT ensemble last for 10 ps with a time step of 1.0 fs and the temperature was controlled by Nosé-Hoover method [32].

To investigate the adsorption performance of Li, Na and Mg atom on Ca_2NOH and $Y_2C(OH)_2$ surfaces, the adsorption energies metal atom on surface are calculated [33,34]. Moreover, PDOS, charge density difference and Bader charge analysis have been calculated to study the charge transfer between the surfaces and metal atoms.

3. Results and discussion

3.1. Structure and electronic properties of Ca_2NOH and $Y_2C(OH)_2$ monolayers

On monolayered Ca_2N/Y_2C surface, three positions for OH group are considered, including on top of the Ca/Y atom (T_1), on top of the C/N atom (T_2) or occupying the hollow center site of Ca/C atoms (H), as shown in Fig. S1. In consideration of the elemental stoichiometric ratio, OH groups may distribute on the same side or on two different sides in the Ca_2NOH structure. Firstly, we calculated the total energies of Ca_2NOH unit cells with OH located at the same surface of Ca_2N slab and the results show that OH groups prefer to occupy the H sites. Afterwards, OH groups spreading on two different sides of Ca_2N surface are investigated and their optimized structures are shown at the bottom of Fig. S1. Calculation results demonstrate that in the most stable Ca_2NOH structure presented as Type II in Fig. S1, OH groups are distributed at two opposite sides. After imposing symmetry, the Ca_2NOH monolayer of Type II is transfer into yz (bc) plane as shown in Fig. 1(a)

and (b). This monolayer is crystallized in P21/M symmetry and its unit cell is composed of four Ca toms, two N atoms and two OH groups with lattice constants of b = 3.559 Å and c = 6.234 Å. For $Y_2C(OH)_2$, two OH groups should locate at the opposite sides in each unit cell and six different configurations in Fig. S2 are considered. The preferential sites for OH groups are also H sites and the most stable geometry for $Y_2C(OH)_2$ is determined to be Type III as shown in Figs. S2 and 1(c) and (d). Its lattice symmetry is $P\bar{3}M1$, in agreement with that of $[Y_2C]^{2+}\cdot 2e^-$. Each $Y_2C(OH)_2$ unit cell includes two Y atoms, one C atom and one OH group and the lattice constants are a = b = 3.550 Å. Moreover, Table S1 summarizes the bond lengths of Ca_2NOH and $Y_2C(OH)_2$.

Their kinetic stability is verified by the fact that there are no appreciable imaginary frequencies in phonon dispersion curves, as shown in Fig. S3(a) and (b). The highest phonon frequencies at G point are 3794.5 cm^{-1} and 3763.8 cm^{-1} and the corresponding Debye temperature are 5461 K and 5417 K for Ca_2NOH and $Y_2C(OH)_2$ respectively, higher than those of graphene and C_3N [35,36]. Moreover, the thermodynamic stability of Ca_2NOH and $Y_2C(OH)_2$ was assessed through MD calculations, in which supercells consisting of 150 and 112 atoms were employed for Ca_2NOH and $Y_2C(OH)_2$, respectively. MD results reveal that the structures remain the lattice constructions at 300 K for 10 ps (Fig. S3(c) and (d)), meaning that Ca_2NOH and $Y_2C(OH)_2$ are thermodynamically stable at room temperature.

The electronic band structure and density of states (DOS) are shown in Fig. 2. Based on HSE06 calculations, the Ca_2NOH monolayer is a semiconductor with an indirect band gap of 1.51 eV, which is appropriate for photocatalysis, solar cell and other photoelectric fields [37,38], while $Y_2C(OH)_2$ monolayer possesses a direct band gap of 0.72 eV. The PDOS results show that valence band maximum of $Ca_2NOH/Y_2C(OH)_2$ is mainly originated from the electrons of Ca/Y atoms, while the corresponding conduction band minimum is mainly from the hybrid states of Ca/Y and N/C atoms. In comparison with the metallic characters of Ca_2N and Y_2C monolayer, the influence of OH groups on the electronic properties is significant. The band gap opening is originated from the decrease of the density of electron cloud near the Fermi level caused by the OH groups.

3.2. The adsorption performance of metal atoms on Ca_2NOH and $Y_2C(OH)_2$ surfaces

Here, the promising application of Ca_2NOH and $Y_2C(OH)_2$ in Li-, Na- and Mg-batteries has been investigated. We firstly studied the adsorption configurations of Li, Na and Mg atoms on Ca_2NOH and $Y_2C(OH)_2$ surfaces. In the calculations, 1 × 3 × 2 and 3 × 3 × 1 supercells are applied for Ca_2NOH and $Y_2C(OH)_2$, respectively and several adsorption sites represented by integers are considered as shown in Fig. S4(a) and (b). Total energy calculations demonstrate that all the three atoms prefer to anchor on Ca_2NOH surface through bonding to O atoms, occupying the site on top of N atom (Site 1), with adsorption energies of −2.01 eV, −1.09 eV and −0.65 eV, respectively. While on $Y_2C(OH)_2$ surface, the adsorption energies for Li, Na and Mg are successively calculated to be −1.96 eV, −1.06 eV and −1.03 eV. And metal atoms are located at the hollow center sites of OH groups (Site 1). These relative high adsorption energies indicate that Ca_2NOH and $Y_2C(OH)_2$ monolayers are appropriate hold materials for Li, Na and Mg atoms. In addition, the distances between alkali metal atoms and O atoms were determined and listed in Table S2.

As can be seen from the charge density difference plots in Fig. 3, there are obvious charge transfer from metal atoms to Ca_2NOH and $Y_2C(OH)_2$ surfaces and the net transferred charges are listed in Table S2. The results show that the interaction between metal atoms and surfaces is Li > Mg > Na. A noteworthy fact is that the transferred electrons are not just located on the surface, but they are distributed within a certain distance from the surface, which is obvious for the cases of metal atoms on Ca_2NOH surface and Mg atom on $Y_2C(OH)_2$ surface. It may be originated from the surface electric field which pulls out the electrons from the surface [20]. PDOS calculations for Ca_2NOH and $Y_2C(OH)_2$ surface before and after adsorption have also been performed [39]. After metal atom adsorption, the band gaps of Ca_2NOH and $Y_2C(OH)_2$ are almost unaffected while new electron states are introduced near the Fermi level (Fig. 4). The amplified PDOS curves near Fermi level are presented in Fig. S5.

The charge and discharge rate of metal ion batteries is closely related to the energy barriers of metal atom diffusion on hold materials and low diffusion barriers are desired [2,40,41]. So diffusion properties of Li, Na and Mg atoms on Ca_2NOH and $Y_2C(OH)_2$ surfaces were further investigated through Nudged Elastic band method and the diffusion paths are presented in Fig. 5. Moreover, the diffusion coefficients (D) of Li, Na and Mg atoms on the two monolayers can be obtained based on the Green–Kubo theory: $D = ga^2\upsilon^* \exp(-E_a/K_BT)$, where g is the reciprocal of possible jump directions, a is the jump distance, E_a is the diffusion barrier and υ^* is the attempt frequency which can be deduced from phonon calculations [42,43]. In consideration of the lattice symmetry of monolayers, two diffusion paths were studied on Ca_2NOH while only one path on $Y_2C(OH)_2$, those are the metal atoms diffusion from one stable adsorption site to another, as shown in Fig. S4.

The obtained diffusion barriers along Path 1 for Li, Na and Mg

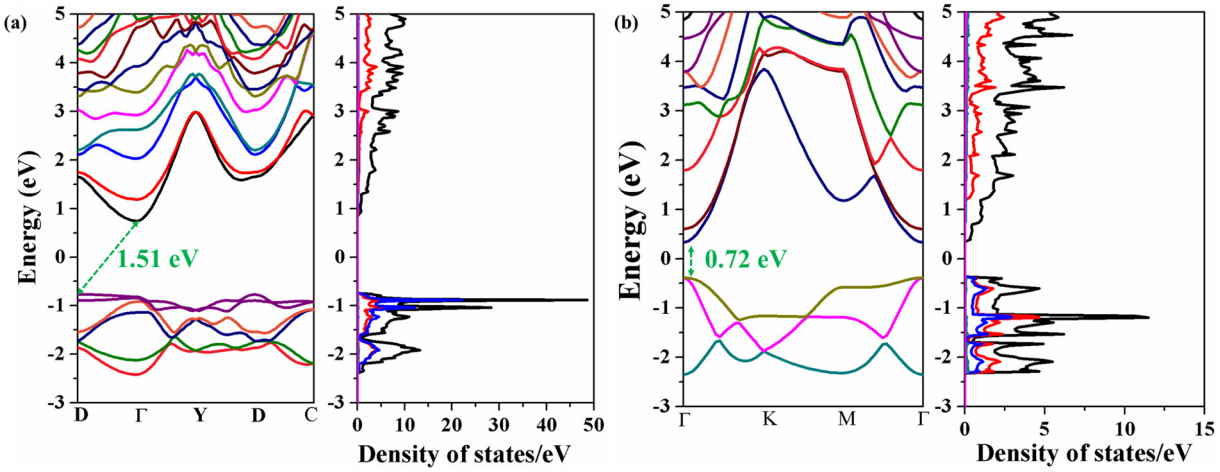

Fig. 2. Calculated band structures and density of states (DOS) for (a) Ca_2NOH and (b) $Y_2C(OH)_2$ monolayer. In the partial density of states (PDOS) plots, the black curves are total density of states. The red curves are the PDOS of Ca/Y atoms and the blue lines indicate the PDOS of N/C atoms. The cyan and pink lines represent the PDOS of O and H atoms, respectively, whose values are relative low in the given energy interval.

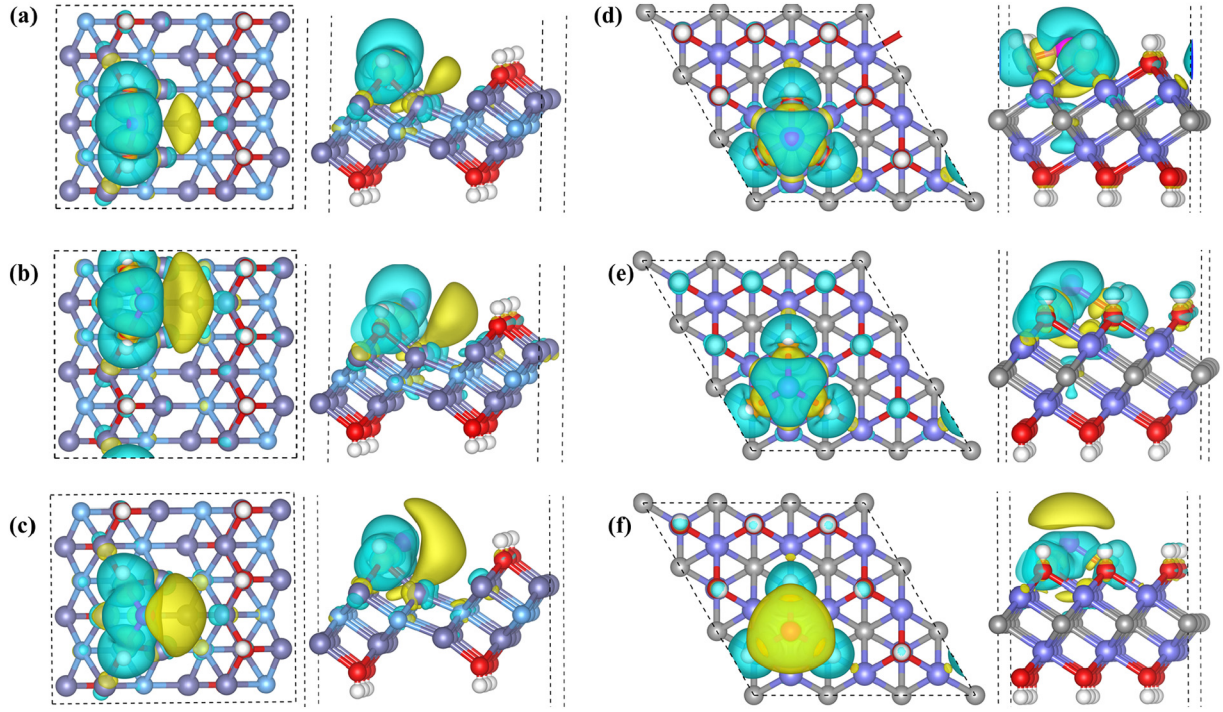

Fig. 3. The isosurface of the difference charge density, the blue (yellow) wireframes denote loss (gain) of electrons. (a) Li, (b) Na and (c) Mg atom adsorbed towards Ca_2NOH surface. (d) Li, (e) Na and (f) Mg atom adsorbed towards $Y_2C(OH)_2$ surface.

atoms on Ca_2NOH surface are 0.78 eV, 0.43 eV and 0.43 eV respectively, lower than those along path 2 (Li: 1.31 eV, Na: 0.60 eV, Mg: 0.68 eV). The calculated attempt frequencies for Li, Na and Mg diffusion along path 1 are respectively 1.66×10^{13}, 1.27×10^{13} and $1.58 \times 10^{13}\,s^{-1}$, all of them are in the range of the usually assumed values (10^{12}–$10^{13}\,s^{-1}$). And their corresponding diffusion coefficients are 2.99×10^{-20}, 4.47×10^{-14}, and $3.23 \times 10^{-14}\,m^2/s$. Obviously, though the relative high adsorption energy of Li atom on Ca_2NOH surface, its big diffusion barriers and diffusion coefficient indicate that Ca_2NOH may not be suitable electrode of Li ion batteries. However, the advisable energy barriers and diffusion coefficients for Na and Mg mean that Ca_2NOH could be possible electrode for Na and Mg ion batteries.

For $Y_2C(OH)_2$ case, it's clearly that the diffusion barrier for Li atom is still the highest, determined as 0.68 eV. While, the diffusion barriers for Na and Mg atom are only 0.27 eV and 0.10 eV respectively. Especially for Mg atom, its predicted diffusion energy barrier of 0.10 eV on $Y_2C(OH)_2$ surface is the lowest according to the reports [44,45]. What's more, the attempt frequencies of Li, Na and Mg are 3.04×10^{13}, 1.28×10^{13} and $2.65 \times 10^{13}\,s^{-1}$, respectively and their diffusion coefficients are 1.52×10^{-18}, 1.52×10^{-12} and $1.52 \times 10^{-8}\,m^2/s$. These results suggest that Na and Mg atoms may diffuse fast on $Y_2C(OH)_2$ monolayer, ensuring high charge and discharge rate of Na/Mg ion batteries. The lower diffusion barriers and large diffusion coefficients of Na and Mg atom may be originated to the weaker interaction between Na/Mg atom and $Ca_2NOH/Y_2C(OH)_2$ surface than that for Na case.

4. Conclusions

In summary, motivated by 'element substitution strategy', the anionic electrons of monolayered electrides were replaced by hydroxyl ions and Ca_2N and Y_2C monolayers were stabilized through the method.

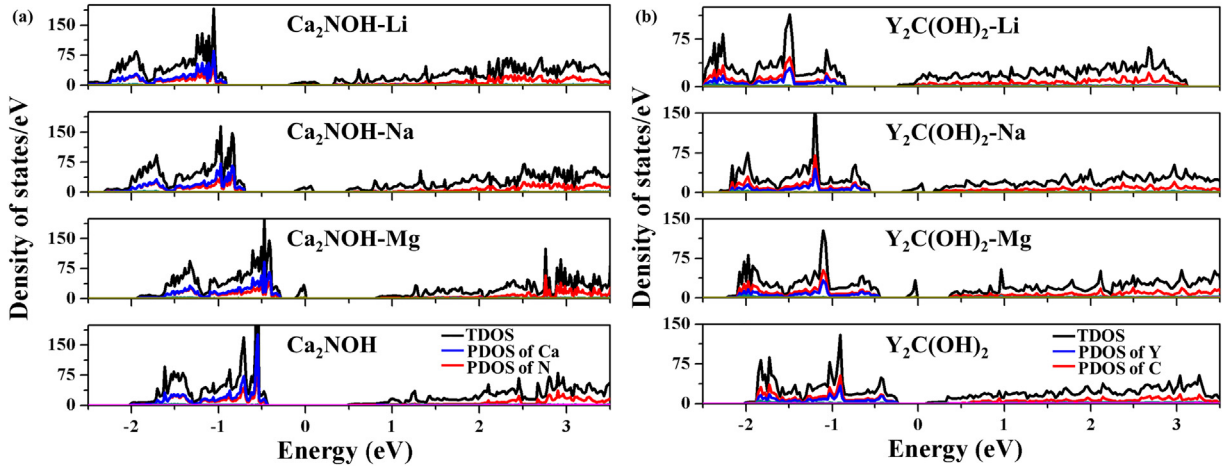

Fig. 4. PDOS plots of metal atoms anchoring on (a) Ca_2NOH surface, and (b) $Y_2C(OH)_2$ surface. The black, red and blue lines denote total DOS, PDOS of Ca/Y atoms and PDOS of N/C atoms, respectively. The amplified PDOS curves near Fermi level are presented in Fig. S3.

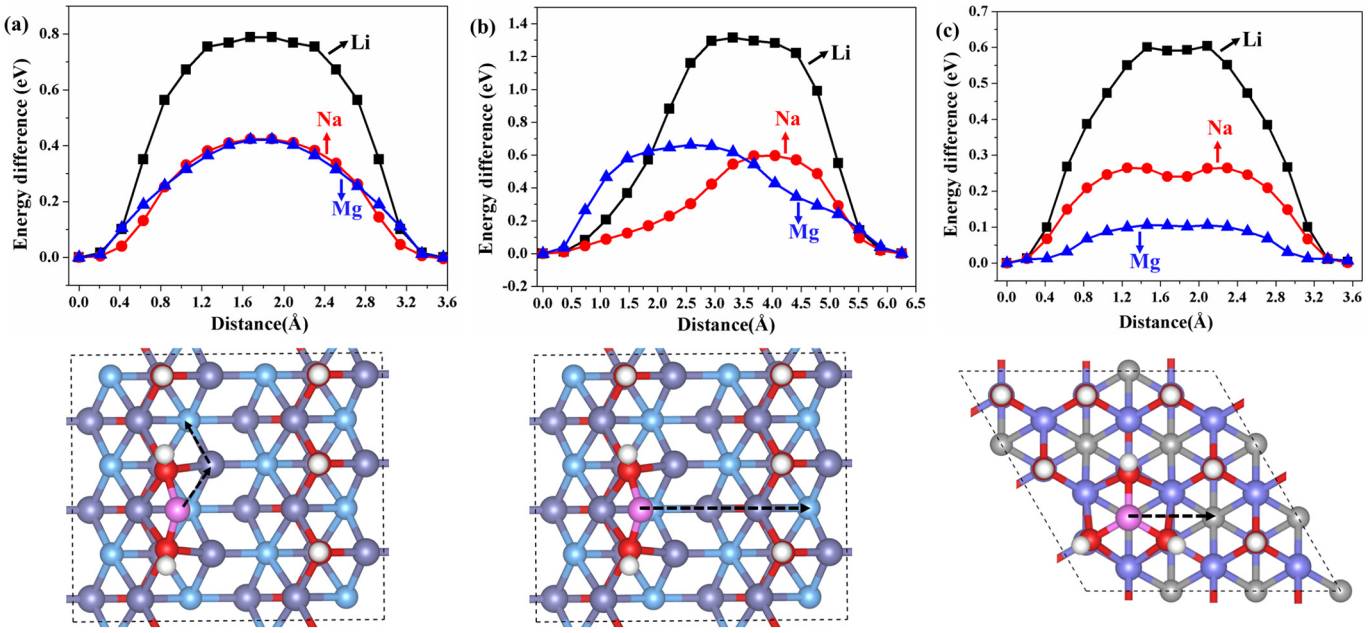

Fig. 5. The diffusion profiles obtained through NEB method for Li, Na and Mg atoms (a) along path 1 on Ca_2NOH surface, (b) along path 2 on Ca_2NOH surface, and (c) along path on $Y_2C(OH)_2$ surface. The black, red and blue lines are respectively for Li, Na and Mg diffusion. The diffusion paths are illustrated by the dotted arrows as shown in the lattice diagrams at the bottom. On Ca_2NOH surface, Path 1 corresponds to metal atom movement passing through the on top site of Ca atom (out of alignment), while in Path 2 metal atoms go directly along a straight line.

Ca_2NOH and $Y_2C(OH)_2$ monolayers were confirmed to be dynamic and thermodynamic stable. Ca_2NOH was identified as indirect semiconductor with a band gap of 1.51 eV while $Y_2C(OH)_2$ possesses a direct band gap of 0.72 eV based on HSE06 calculations. Li, Na and Mg atoms could anchor on Ca_2NOH and $Y_2C(OH)_2$ surfaces. NEB results suggest that those three metal atoms could diffuse with low energy barriers. The barriers for Li, Na, and Mg diffusion on Ca_2NOH surface are 0.79 eV, 0.42 eV and 0.42 eV. While on $Y_2C(OH)_2$ surface, the barriers are lower, 0.60 eV, 0.26 eV and 0.10 eV for Li, Na and Mg, respectively and their corresponding diffusion coefficients are as large as 1.52×10^{-18}, 1.52×10^{-12} and 1.52×10^{-8} m^2/s. The diffusion barriers and diffusion coefficients for Na and Mg atoms indicate that Ca_2NOH and $Y_2C(OH)_2$ monolayers are suitable electrode materials for corresponding metal ion batteries. All the results serve to design novel 2D materials and employ their properties in some applications.

Acknowledgments

This work was supported by NSFC, China (11604330, 21622509, 21475122, 21527806), Department of Science and Technology of Jilin Province (20160201008GX), Jilin Province Development and Reform Commission (2016C014 and 2017C053-1), Changchun Science and Technology Bureau (15SS05).

Appendix A. Supplementary data

Supplementary data to this article can be found online at https://doi.org/10.1016/j.apsusc.2019.01.256.

References

[1] M. Autore, P. Li, I. Dolado, F.J. Alfaro-Mozaz, R. Esteban, A. Atxabal, F. Casanova, L.E. Hueso, P.A. Alonso-González, J. Aizpurua, A.Y. Nikitin, S. Vélez, R. Hillenbrand, Boron nitride nanoresonators for phonon-enhanced molecular vibrational spectroscopy at the strong coupling limit, Light Sci. Appl. 7 (2018) 17172.
[2] Q. Tang, Z. Zhou, P. Shen, Are MXenes promising anode materials for Li ion batteries? Computational studies on electronic properties and Li storage capability of Ti3C2 and Ti3C2X2 (X = F, OH) monolayer, J. Am. Chem. Soc. 134 (2012) 16909–16916.
[3] J. Kibsgaard, Z.B. Chen, B.N. Reinecke, T.F. Jaramillo, Engineering the surface structure of MoS_2 to preferentially expose active edge sites for electrocatalysis, Nat. Mater. 11 (2012) 963–969.
[4] V. Apalkov, M.I. Stockman, Proposed graphene nanospaser, Light Sci. Appl. 3 (2014) e191.
[5] K. Lee, S.W. Kim, Y. Toda, S. Matsuishi, H. Hosono, Dicalcium nitride as a two-dimensional electride with an anionic electron layer, Nature 494 (2013) 336–341.
[6] D.L. Druffel, K.L. Kuntz, A.H. Woomer, F.M. Alcorn, J. Hu, C.L. Donley, S.C. Warren, Experimental demonstration of an electride as a 2D material, J. Am. Chem. Soc. 138 (2016) 16089–16094.
[7] J.S. Oh, C.J. Kang, Y.J. Kim, S. Sinn, M. Han, Y.J. Chang, B.G. Park, S.W. Kim, B.I. Min, H.D. Kim, T.W. Noh, Evidence for anionic excess electrons in a quasi-two-dimensional Ca_2N electride by angle-resolved photoemission spectroscopy, J. Am. Chem. Soc. 138 (2016) 2496–2499.
[8] J. Park, K. Lee, S.Y. Lee, C.N. Nandadasa, S. Kim, K.H. Lee, Y.H. Lee, H. Hosono, S.-G. Kim, S.W. Kim, Strong localization of anionic electrons at interlayer for electrical and magnetic anisotropy in two-dimensional Y_2C electride, J. Am. Chem. Soc. 139 (2017) 615–618.
[9] H.Q. Huang, K.H. Jin, S.H. Zhang, F. Liu, Topological electride Y_2C, Nano Lett. 18 (2018) 1972–1977.
[10] W. Ming, M. Yoon, M.H. Du, K. Lee, S.W.J. Kim, Am. Chem. Soc. 138 (2016) 15336–15344.
[11] T. Tada, S. Takemoto, S. Matsuishi, H. Hosono, Inorg. Chem. 53 (2014) 10347–10358.
[12] Y.J. Kim, S.M. Kim, H. Hosono, J.W. Yang, S.W. Kim, The scalable pinacol coupling reaction utilizing the inorganic electride $[Ca_2N]^+e^-$ as an electron donor, Chem. Commun. 50 (2014) 4791–4794.
[13] J. Hu, B. Xu, S.A. Yang, S. Guan, C. Ouyang, Y. Yao, 2D electrides as promising anode materials for Na-ion batteries from first-principles study, ACS Appl. Mater. Interfaces 7 (2015) 24016–24022.
[14] J.H. Hou, K.X. Tu, Z.F. Chen, Two-dimensional Y2C electride: a promising anode material for Na-ion batteries, J. Phys. Chem. C 120 (2016) 18473–18478.
[15] G. Chen, Y. Bai, H. Li, Y. Li, Z. Wang, Q. Ni, L. Liu, F. Wu, Y. Yao, C. Wu, Multilayered electride Ca_2N electrode via compression molding fabrication for sodium ion batteries, ACS Appl. Mater. Interfaces 9 (2017) 6666–6669.
[16] M.J. Sharif, M. Kitano, Y. Inoue, Y. Niwa, H. Abe, T. Yokoyama, M. Hara, H. Hosono, Electron donation enhanced CO oxidation over Ru-loaded $12CaO{\cdot}7Al_2O_3$ electride catalyst, J. Phys. Chem. C 119 (2015) 11725–11731.
[17] M. Kitano, Y. Inoue, Y. Yamazaki, F. Hayashi, S. Kanbare, S. Matsuishi, T. Yokoyama, S.W. Kim, M. Hara, H. Hosono, Nat. Chem. 4 (2012) 934–940.
[18] B. Mortazavi, G.R. Berdiyorov, M. Shahrokhi, T. Rabczuk, Mechanical, optoelectronic and transport properties of single-layer Ca_2N and Sr_2N electrides, J. Alloys Compd. 739 (2018) 643–652.
[19] S. Guan, S.A. Yang, L.Y. Zhu, J.P. Hu, Y.G. Yao, Electronic, dielectric, and plasmonic properties of two-dimensional electride materials X_2N (X = Ca, Sr): a first-principles study, Sci. Rep. 5 (2015) 12285.
[20] Y. Oh, J. Lee, J. Park, H. Kwon, I. Jeon, S.W. Kim, G. Kim, S. Park, S.W. Hwang, Electric field effect on the electronic structure of 2D Y2C electride, 2D Mater. 5 (2018) 035005.

[21] S.T. Zhao, Z.Y. Li, J.L. Yang, Obtaining two-dimensional electron gas in free space without resorting to electron doping: an electride based design, J. Am. Chem. Soc. 136 (2014) 13313–13318.
[22] S.R. Lingampalli, K. Manjunath, S. Shenoy, U.V. Waghmare, C.N.R. Rao, Zn2NF and related analogues of ZnO, J. Am. Chem. Soc. 138 (2016) 8228–8234.
[23] D.D. Wang, Z.H. Sun, D.X. Han, L. Liu, L. Niu, Ti3BN monolayer: the MXene-like material predicted by first-principles calculations, RSC Adv. 7 (2017) 11834–11839.
[24] P. Hohenberg, K. Walter, Inhomogeneous electron gas, Phys. Rev. 136 (1964) B864–B871.
[25] G. Kresse, D. Joubert, From ultrasoft pseudopotentials to the projector augmented-wave method, Phys. Rev. B 59 (1999) 1758.
[26] J.P. Perdew, K. Burke, M. Ernzerhof, Generalized gradient approximation made simple, Phys. Rev. Lett. 77 (1996) 3865.
[27] J. Heyd, G.E. Scuseria, M. Ernzerhof, Hybrid functionals based on a screened Coulomb potential, J. Chem. Phys. 118 (2003) 8207–8215.
[28] S. Grimme, Semiempirical GGA-type density functional constructed with a long-range dispersion correction, J. Comput. Chem. 27 (2006) 1787.
[29] S. Baroni, P. Giannozzi, A. Testa, Green-function approach to linear response in solids, Phys. Rev. Lett. 58 (1987) 1861.
[30] X. Gonze, Perturbation expansion of variational-principles at arbitrary order, Phys. Rev. A 52 (1995) 1086.
[31] M.C. Payne, M.P. Teter, D.C. Allan, T.A. Arias, J.D. Joannopoulos, Iterative minimization techniques for ab initio total-energy calculations-molecular-dynamics and conjugate gradients, Rev. Mod. Phys. 64 (1992) 1045–1097.
[32] G.J. Martyna, M.L. Klein, M.E. Tuckerman, Nose-Hoover chains-the canonical ensemble via continuous dynamics, J. Chem. Phys. 97 (1992) 2635–2643.
[33] O.I. Malyi, V.V. Kulish, T.L. Tan, S. Manzhos, A computational study of the insertion of Li, Na, and Mg atoms into Si(111) nanosheets, Nano Energy 2 (2013) 1149–1157.
[34] O.I. Malyi, K. Sophiha, V.V. Kulish, T.L. Tan, S. Manzhos, C. Persson, A computational study of Na behavior on graphene, Appl. Surf. Sci. 333 (2015) 235–243.
[35] P. Eric, V. Vikas, K.R. Ajit, Thermal properties of graphene: fundamentals and applications, MRS Bull. 37 (2012) 1273.
[36] D.D. Wang, Y. Bao, T.S. Wu, S.Y. Gan, D.X. Han, L. Niu, First-principles study of the role of strain and hydrogenation on C3N, Carbon 134 (2018) 22–28.
[37] D.W. Shao, L.C. Zheng, D.Q. Feng, J. He, R. Zhang, H. Liu, X.H. Zhang, Z.M. Lu, W.C. Wang, W.H. Wang, F. Lu, H. Dong, Y.H. Cheng, H. Liu, R.K. Zheng, TiO_2–P3HT:PCBM photoelectrochemical tandem cells for solar-driven overall water splitting, J. Mater. Chem. A 6 (2018) 4032–4039.
[38] H. Zhang, H. Wang, H.M. Zhu, C.C. Chueh, W. Chen, S.H. Yang, A.K.Y. Jen, Low-temperature solution-processed $CuCrO_2$ hole-transporting layer for efficient and photostable perovskite solar cells, Adv. Energy Mater. 8 (2018) 1702762.
[39] J. Hu, W. Chen, X. Zhao, H.B. Su, Z. Chen, The anisotropy properties of electronic, adsorption and stability of low-index BiVO4 surfaces for photoelectrochemical applications, ACS Appl. Mater. Interfaces 10 (2018) 5475–5484.
[40] C.H. Sun, X.H. Yang, J.S. Chen, Z. Li, X.W. Lou, C. Li, S.C. Smith, G.Q. Lu, H.G. Yang, Higher charge/discharge rates of lithium-ions across engineered TiO_2 surfaces leads to enhanced battery performance, Chem. Commun. 46 (2010) 6129–6131.
[41] K. Persson, Y. Hinuma, Y.S. Meng, A. Van der Ven, G. Ceder, Thermodynamic and kinetic properties of the Li-graphite system from first-principles calculations, Phys. Rev. B 82 (2010) 125416.
[42] G. Yoon, D.-H. Kim, I. Park, D. Chang, B. Kim, B. Lee, K. Oh, K. Kang, Using first-principles calculations for the advancement of materials for rechargeable batteries, Adv. Funct. Mater. 10 (2017) 1702887.
[43] J. Koettgen, T. Zacherle, S. Grieshammer, M. Martin, Ab initio calculations of the attempt frequency of oxygen diffusion in pure and samarium doped ceria, Phys. Chem. Chem. Phys. 19 (2017) 9957–9973.
[44] X. Ji, J. Chen, F. Wang, W. Sun, Y.J. Ruan, L. Miao, J.J. Jiang, C.S. Wang, Water-activated $VOPO_4$ for magnesium ion batteries, Nano Lett. (2018), https://doi.org/10.1021/acs.nanolett.8b02854.
[45] T.A. Barnes, L.F. Wan, P.R.C. Kent, D. Prendergast, Hybrid DFT investigation of the energetics of Mg ion diffusion in MoO_3, Phys. Chem. Chem. Phys. (2018), https://doi.org/10.1039/C8CP05511D.